Check for updates

# Dynamics analysis and fractional-order nonlinearity system via memristor-based Chua oscillator

S SABARATHINAM[1], VIKTOR PAPOV[1], ZI-PENG WANG[2,3,4], R VADIVEL[5] and NALLAPPAN GUNASEKARAN[6,7] [iD],*

[1]Laboratory of Complex Systems Modelling and Control, Faculty of Computer Science, National Research University, HSE Moscow, Russia
[2]Beijing Key Laboratory of Computational Intelligence and Intelligent System, Beijing University of Technology, Beijing 100124, China
[3]Beijing Institute of Artificial Intelligence, Beijing University of Technology, Beijing 100124, China
[4]Beijing Laboratory of Smart Environmental Protection, Beijing University of Technology, Beijing 100124, China
[5]Department of Mathematics, Faculty of Science and Technology, Phuket Rajabhat University, Phuket 83000, Thailand
[6]Computational Intelligence Laboratory, Toyota Technological Institute, Nagoya 468-8511, Japan
[7]Eastern Michigan Joint College of Engineering, Beibu Gulf University, Qinzhou 535011, China
*Corresponding author. E-mail: gunasmaths@gmail.com

**Abstract.** This article discusses the utilisation of a Chua oscillator with a memristor to produce chaos with minimal nonlinearity. The memristor, a device that changes its flux or charges over time, has its nonlinear strength altered fractionally to determine the lowest-order memristor nonlinearity for generating chaos. An experimental analog circuit in real-time has been constructed. A linear parameter varying (LPV) approach, incorporating a suitable Lyapunov functional (LK) method, has been introduced to find new sufficient conditions for the robust stability of the resulting closed-loop system through linear matrix inequalities (LMIs). By observing the behaviour of the system without control, it is possible to understand the basic characteristics of chaotic oscillations and how they are affected by changes in the fractional order. These results can then be used as a starting point to study the effectiveness of various control techniques, such as feedback control, in reducing chaos and stabilising the system of this article. The efficiency of the cost-function-based control scheme is evaluated using the simulation results and relevant applications are addressed.

## 1. Introduction

Resistance, capacitance and inductance are the three basic circuit components in passive circuit theory. The fourth passive circuit element, namely 'memristor', is a breakthrough in the field of fundamental electronics theory because of its memory property [1–6]. The memristor concept is widely understood by the state-dependent Ohm's law, i.e., the resistive property of the memristor element which depends on the state variable (history property) of the memristor system [7–9]. Studying memristor-based nonlinear systems with different forms of nonlinearity such as piecewise [10], cubic [11], tanh [12] has been very fruitful in recent years. Generally, the memristor's nonlinearity differs from that of the classical nonlinear elements because, when the memristor-based system is constructed, one additional dimension is added to the system mathematical equation because of the memristor property (rate of change of flux/charge) and the memristor has potential applications in electronics circuits because of its nonlinearity as well as memory properties [13,14]. Another advantage is that the resistance and the conductance of the memristor profile can be adjustable [15,16]. Recently,

the construction of memristor-based dynamical systems from classical systems is getting more attention [17–19]. Moreover, the concept of various types of memristive neural networks (MNNs) has been widely employed in numerous sectors and the memristor is recognised as an outstanding circuit element which mimics artificial neural network synapses. This has drawn a lot of interest from researchers [20].

In the domains of dynamical systems and control theory, a fractional-order system is a dynamical system that can be modelled by a fractional differential equation having derivatives of non-integer order. Such systems are called fractional-order systems which hereafter are called FO. Derivatives and integrals of fractional orders are used to describe objects that can be characterised by power-law non-locality, power-law long-range dependence or fractal properties. The importance of FO dynamical systems has become a subject of great interest in several fields of differential and integral computing [21,22]. The implementation of FO dynamical systems has been well-established in recent years. Moreover, it becomes an emerging topic in science and engineering [22–25]. The fractional-order derivatives and integrals are present especially in electronics [26], telecommunications [27], automatic control [28], etc. For more details on the importance of fractional-order-based neural network, see [29] and for the memristor-based fractional neural network, see [30]. The novelty of this work is that the memristor-based system can be converted to FO.

On the other hand, there are several reports on FO for answering the question: "What is the minimum dimension/order for obtaining chaos?" (see [31,32] and references therein). But in the present manuscript, the main question is "What is the minimum order of (strength) nonlinearity to obtain chaos?". In this paper, the order of flux/charge (which causes the non-linear strength) is varied to obtain chaos. Notice that in classical dynamical systems, the nonlinear strength cannot be varied fractionally. To the best of our knowledge, this is the first study, where the fractional nonlinearity of the memristor-based dynamical systems is studied.

The second part of the manuscript studies controlling the chaos in our proposed FO. In addition, studies that were using memristors in the area of control frameworks have become far and wide in the past years. It is important to establish control systems that not only achieve stability over time, but also ensure a satisfactory level of system performance. The robustness and execution of FO models have drawn many researchers, with spotlight on the stability of FO uncertain systems. Towards the end of the last few years, we have found extensive exploration of the stability and stabilisation of general FO frameworks with different control procedures [33,34].

One way to deal with this issue is the supposed guaranteed cost control approach which was first presented by Chang and Peng in 1972. This methodology gives an upper bound on the execution list of a given system and subsequently, the degradation of the system execution caused by the uncertainties is guaranteed to be less than this bound. The linear matrix inequality (LMI)-based approach has been among the famous and popular ones to study the issue of guaranteed cost control of the FO systems and some significant outcomes can be seen in [35–40]. Specifically, output-feedback-guaranteed cost control of FO uncertain linear delayed systems is discussed in [35]. Thuan and Huong [41] studied robust guaranteed cost control of FO neural network systems with time delays. It is significant to note that research on the dynamic behaviour of LPV with an FO system plays an important role both in theory and application [42–44]. Yet, as we know, no study has been done to tackle the LPV with memristive chaotic oscillators of the FO systems.

By employing the Lyapunov functional theory and using a linear parametric varying approach, some adequate conditions are obtained to ensure the robust stability of the addressed system. This can be achieved by solving LMIs, which can be effectively worked with by utilising the standard mathematical programming. Moreover, the optimal robust guaranteed cost controller is inferred on the basis of the LMI approach and, accordingly, the quadratic cost function is determined. Finally, a numerical example is given to show the suitability of the proposed technique. Moreover, the significant contributions of this present study are:

- The guaranteed cost control problem for the least-FO system under uncertainty has been developed.
- By using the Lyapunov stability theory, a new arrangement of adequate conditions has been developed by means of LMIs that guarantees the feasibility of the considered model.
- The guaranteed cost controller with quadratic cost function not only fulfills a specific measure of energy utilisation but additionally guarantees the system stability with an adequate level of execution.
- The desired controllers are obtained by solving the developed LMI constraints. Finally, the importance and benefit of the control law are approved through the numerical example with simulation results.
- The representation of the work flow of the present study is shown as a schematic diagram in figure 1.

The paper is structured as follows. Section 2 gives the structure of the FO derivatives and the construction of the memristor-based systems. The memristor-based fractional Chua oscillator is constructed in §3. The numerical and experimental studies are given in the
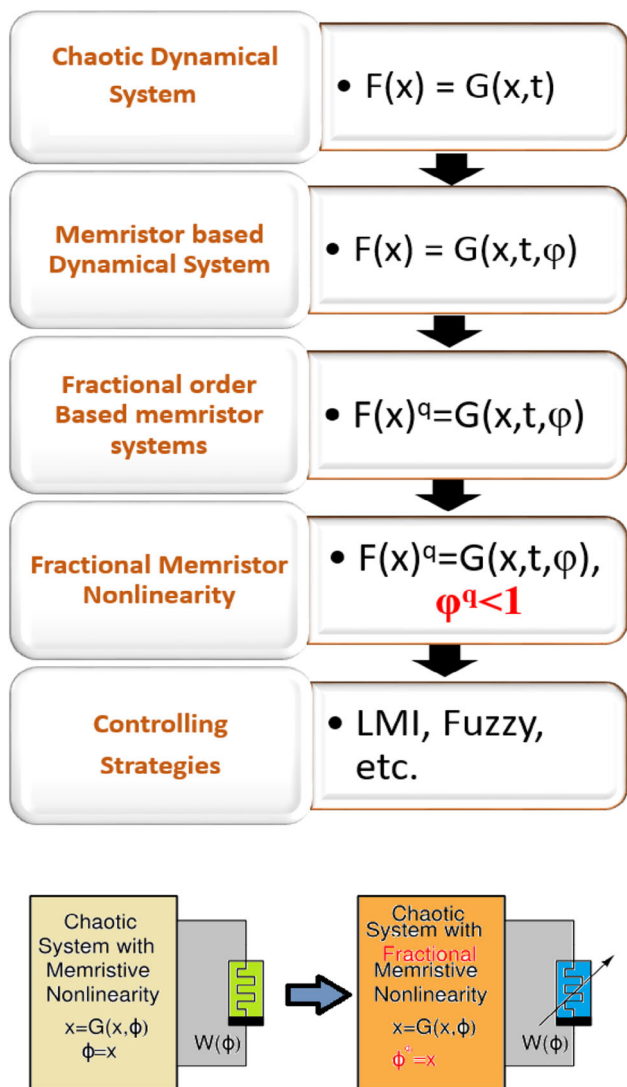
**Figure 1.** (*Upper panel*) Sketch of the work flow of the present study and (*lower panel*) the memristor system transforms to FO nonlinearity memristor-based systems.

same section. The control of oscillation methodologies is discussed in §4 and the controlled numerical results are shown in §5. The importance and possible applications are discussed in §6. Finally, §7 summarises the results.

## 2. Fractional derivatives and integrals

Three general formulations of fractional derivatives proposed to transform integer operators into non-integer operators are available in the literature. The primary purpose of these transformations is to convert non-integer derivatives or integrals of the fractional operator $D_t^q$. However, in the literature, the Grünwald–Letnikov method [45], the Riemann–Liouville method [46] and

the Caputo method [47] are widely used for transformations. The integral operator (continuous) is identified in three categories of formulations, i.e., $D_t^q = d^q/dt^q$, when $q > 0$, $D_t^q = 1$, when $q = 0$ and $D_t^q = \int_0^t (d\tau)^q$, when $q < 0$. In the present study, we use the Riemann–Liouville method to construct fractional derivatives. This formulation is given by

$$_0D_t^q f(t) = \frac{1}{\Gamma(n-q)} \frac{d^n}{dt^n} \int_0^t \frac{f(\tau)}{(t-\tau)^{q-n+1}} d\tau. \quad (1)$$

The Euler gamma function is $\Gamma(\cdot)$ and considered as $(n-1) \leq q < n$. Time $t = 0$, and all initial conditions are considered as zero. Here, the Laplace transform of the fractional derivative formulation Riemann–Liouville can be written as

$$L\left\{\frac{d^q f(t)}{dt^q}\right\} = S^q L\{f(t)\}. \quad (2)$$

Notice that the fractional derivative order is described by $q$. The operator $q$ is the transfer function written in frequency domain, that is, $F(s) = 1/S^q$. The definitions of fractional integral do not permit direct execution of the operator of intricate systems with fractional elements in time-domain simulations. It is important to create approximations for the fractional operators using the traditional integer-order operators to investigate the system. Linear transfer procedure approximations of the fractional integrator of order 0.1 to 0.9, is established in the frequency domain statements and the resulting counterpart representatives are given in [48–50]. Figure 2d shows the ladder circuit that produces fractional order from 0.9 to 0.1 by varying the resistance and capacitance values.

### 2.1 *Construction of memristor nonlinearity (cubic)*

In general, the memristor is described with two classes of nonlinear constitutive associations between device voltage ($v$) and current ($i$),

$$\begin{cases} v = M(q)i, \\ i = W(\phi)v, \end{cases} \quad (3)$$

where $W(\phi)$ and $M(q)$ are nonlinear functions of flux ($\phi$) and charge ($q$), called as memductance and memristance, respectively [11] and are defined as follows:

$$\begin{cases} M(q) = \dfrac{d\phi(q)}{dq}, \\ W(\phi) = \dfrac{dq(\phi)}{d\phi}. \end{cases} \quad (4)$$

The memristor developed in this study is a charge-controlled memristor represented by the association in eq. (3). The link between the terminal voltage and the

terminal current of the memristor is acquired by

$$
\begin{cases}
v = \dfrac{d\phi}{dt} = \dfrac{d\phi}{dq} \dfrac{dq}{dt} = \dfrac{d\phi}{dq}, & i = M(q)i, \\
i = \dfrac{dq}{dt} = \dfrac{dq}{d\phi} \dfrac{d\phi}{dt} = \dfrac{dq}{d\phi}, & v = W(\phi)v.
\end{cases} \tag{5}
$$

The cubic nonlinearity is considered to transform as a memristor emulator and it is defined as

$$
\begin{cases}
\phi(q) = \xi q + \nu q^3, \\
q(\phi) = \xi \phi + \nu \phi^3.
\end{cases} \tag{6}
$$

The memristance and memductance are connected to the flux and charge as

$$
\begin{cases}
M(q) = \dfrac{d\phi}{dq} = \xi + 3\nu q^2, \\
W(\phi) = \dfrac{dq}{d\phi} = \xi + 3\nu \phi^2.
\end{cases} \tag{7}
$$

Notice that $M(q)$ and $W(\phi)$ are the emulator memristance and memductance emulator, respectively [51]. This cubic nonlinearity transformation is used in this study to construct a memristor-based Chua system.

## 3. Memristor-based Chua oscillator

The memristor-based Chua system is well-known in recent times. The Chua systems based on memristors have four dynamic storage components, i.e., capacitors $C_1$, $C_2$, inductor $L$ and non-ideal active voltage controlled memristor. The corresponding four state variables $v_1$, $v_2$, $i_3$ and $v_0$ are shown in figure 2a. The state equations are written as

$$
\begin{cases}
\dfrac{dv_1}{dt} = \dfrac{1}{RC_1}(v_2 - v_1) + \dfrac{(G_a - G_b v_0^2)v_1}{c_1} \\
\dfrac{dv_2}{dt} = \dfrac{1}{RC_2}(v_1 - v_2) - \dfrac{i_3}{C_2} \\
\dfrac{dv_3}{dt} = \dfrac{v_2}{L} \\
\dfrac{dv_4}{dt} = -\dfrac{v_1}{R_1 c_0} - \dfrac{v_0}{R_2 C_0}.
\end{cases} \tag{8}
$$

In this circuit schematic, the traditional memristor nonlinearity is replaced by the FO memristor in Chua's system (see figures 2c and 2d). For rescaling, parameters in dimensionless forms such as $m = v_1$, $y = v_2$, $z = Ri_3$, $w = v_4$, $\tau = t/(RC_2)$, $a = RC_a$, $b = RG_b$, $\hat{\alpha} = C_2/C_1$, $\beta = R^2 C_2/L$, $\rho = RC_2/R_1 C_0$, $\epsilon = RC_2/R_2 C_0$ and defining a nonlinear function $W(u) = a - bu^2$, the dimensionless state equation is
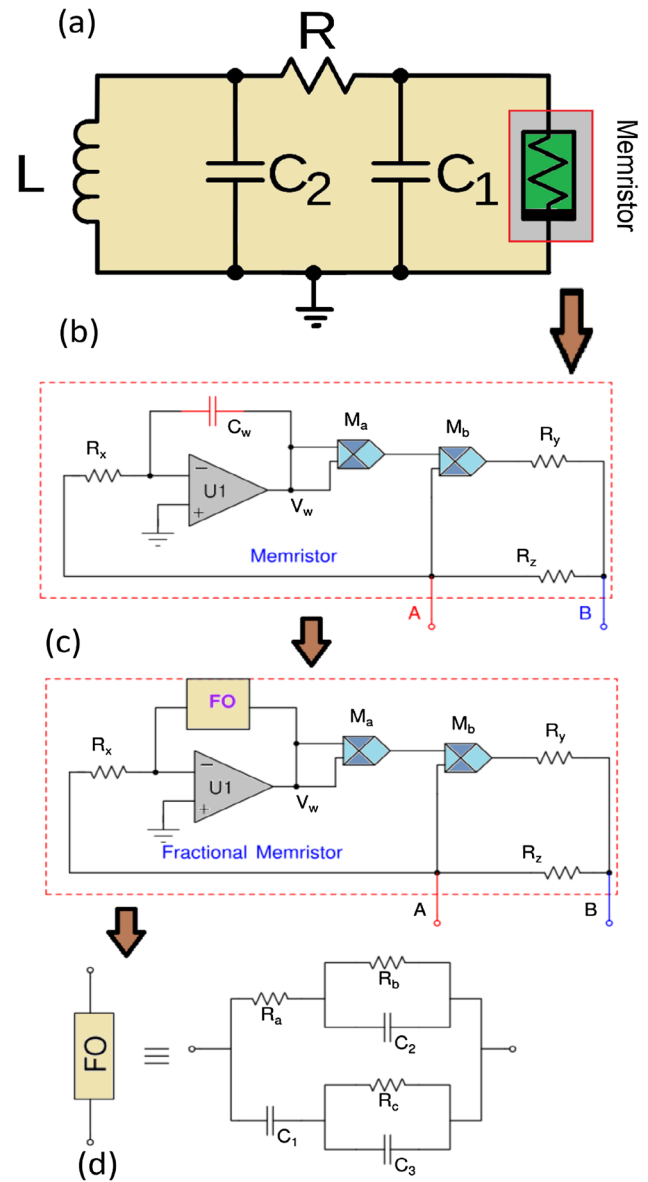


**Figure 2.** (**a**) Schematic diagram of the memristor-based Chua oscillator, (**b**) memristor subcircuit schematic, (**c**) yellow box: memristor replaced with FO and (**d**) the ladder subcircuit of FO.

written as

$$
\begin{cases}
\dot{m} = \hat{\alpha}[y - m + W(w)m] \\
\dot{y} = m - y - z \\
\dot{z} = \beta y \\
\dot{w} = -\rho m - \epsilon w.
\end{cases} \tag{9}
$$

The normalised system parameter is fixed for chaotic oscillation as $\hat{\alpha} = 12$, $\beta = 28$, $\rho = 37$, $\epsilon = 12$, $a = 1.6$, $b = 0.16$. Based on our previous discussion, the fractional-order memristor nonlinearity based on Chua's
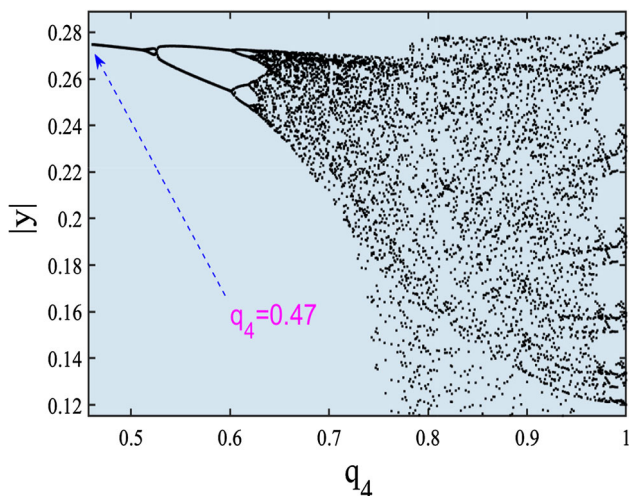
**Figure 3.** Diagram of one-parameter bifurcation in the $(q_4 - |y|)$ plane of (10). $|y|$: maxima of the variable $y$. The system parameter and initial conditions are fixed.

system is written as

$$\begin{cases} \dot{m}^{q_1} = \hat{\alpha}[y - m + W(w)m] \\ \dot{y}^{q_2} = m - y - z \\ \dot{z}^{q_3} = \beta y \\ \dot{w}^{q_4} = -\rho m - \epsilon w, \end{cases} \tag{10}$$

where $q_4$ is fractionally varied and the fractional orders of the system state variables are fixed as $q_1, q_2$ and $q_3 = 1$.

### 3.1 *Numerical and experimental results*

To understand the effect of fractional nonlinearity, system (10) parameters are fixed as exhibiting chaotic oscillations. Figure 3 shows a one-parameter bifurcation diagram with respect to $q_4$. We can see from this bifurcation diagram, that the chaotic attractor exists up to $q_4 = 0.47$, and beyond the FO values, the system has no oscillations. Figure 4 shows different projections of phase portraits in the (a) $m-y$, (b) $m-z$, (c) $m-w$ planes and (ii) time series of $m(t)$, $y(t)$, $z(t)$ state variables at $q_4 = 0.8$.

Figure 5 shows the three-dimensional multibifurcational plot with respect to the system parameter $\hat{\alpha}$ vs. $q_4$. As in the earlier discussion, chaos and oscillation vanished beyond $q_4 = 0.47$. From this multibifurcation plot, we could see that when the fractional order varies, the length of the bifurcation is varied (shifted). The system parameter $\hat{\alpha}$ is varied in the ranges of $\hat{\alpha} \in (6.5, 10)$.
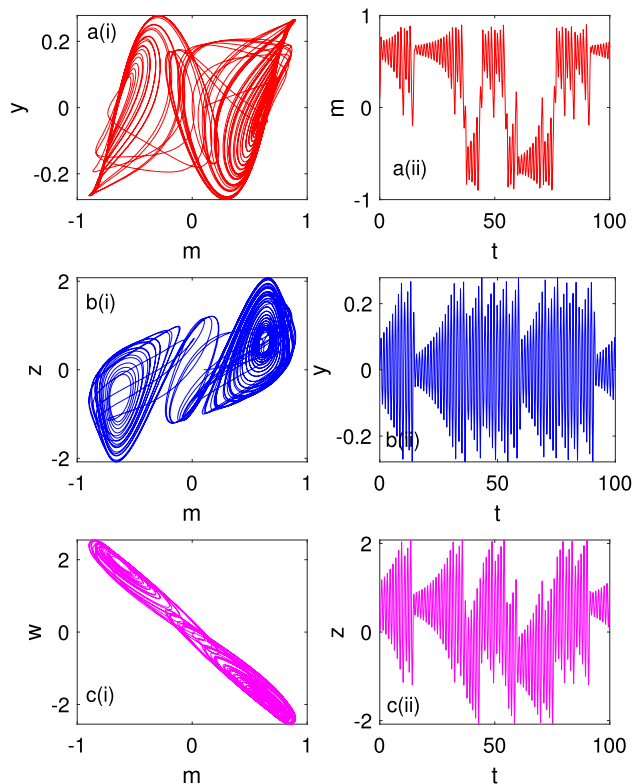


**Figure 4.** Different numerically observed projections of (**i**) phase portrait (**a**) $m-y$, (**b**) $m-z$, (**c**) $m-w$ planes and (**ii**) time series of $m(t)$, $y(t)$, $z(t)$ variables, respectively, at FO $q_4 = 0.8$. The parameter and the initial conditions are fixed.

### 3.2 *Two-parameter scanning*

Figure 6 shows the two-parameter scanning for the separation of chaotic and boundary/no oscillation differentiated using numerical frequencies. In this figure, OS represents the chaotic region, NO represents the zone without oscillation and B represents the boundary of the system. In figure 6, the existence of multistability and the limitation of the chaotic regions are clearly identified. Notice that the other fractional derivative plot $q_3$ vs. $q_4$ are omitted here for the sake of simplicity.

### 3.3 *Multistability*

The term called multistability is generally known as the coexistence of one or more stationary orbits (attractor) that exhibit the same set of system parameters with differences in the initial condition of the system. It has been a very interesting research topic in recent years because it is used fully for modelling a natural process, attracting attention and knowledge about a phase transition, biological diversification, etc. The switching properties of the multistable attractor for different initial conditions or due to the perturbation switching between
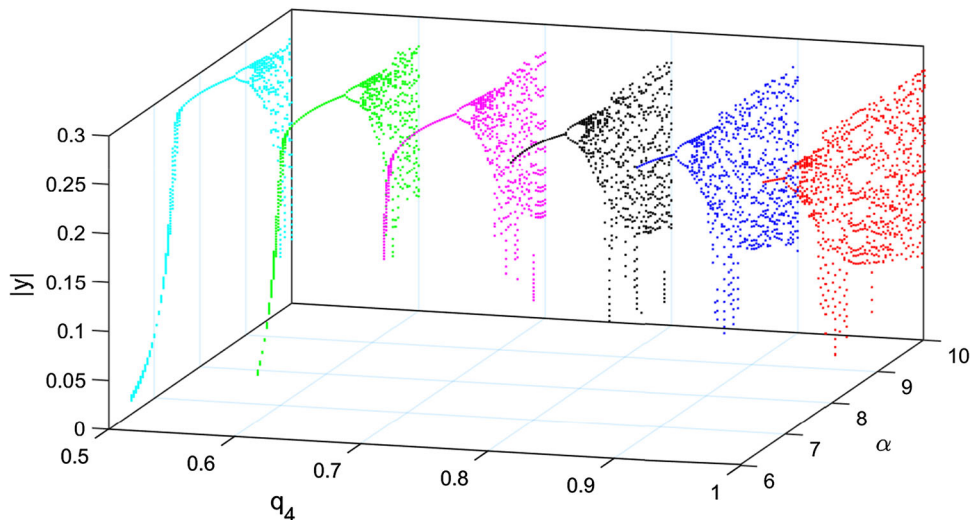
**Figure 5.** Three-dimensional bifurcation diagram with respect to the system parameter $\hat{\alpha}$ vs. $q_4$. The different colours of the bifurcation shows the suppression of oscillation in the $\hat{\alpha}$ regime.
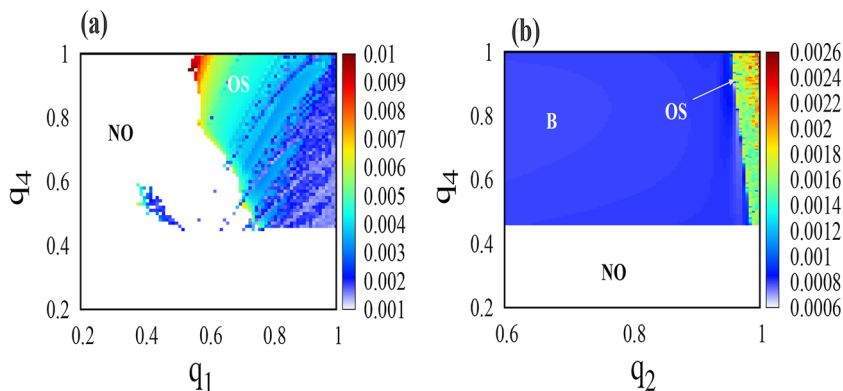


**Figure 6.** Scanning by two parameters of (**a**) $q_1$–$q_4$ and (**b**) $q_2$–$q_4$ fractional-order plane of system (10). The time series frequency is calculated for separating oscillation and no oscillation regimes with respect to $q_1$, $q_2$ and $q_4$

trajectories give more insight into up-to-date technological applications. From the basin plot (ref. [5]) of the earlier section, the multistability is identified by plotting the phase space plots. Figure 7 shows the properties of the symmetry by changing the initial conditions. The blue colour attractor is obtained at $(m^*, x^*, y^*, z^*) = (0.1, 0.3, 0.2, 0)$ and the red colour attractor is obtained at $(m^*, x^*, y^*, z^*) = (0.6, 0.3, 0.2, 0)$. The two different colour symmetry attractors promise the switching properties of the systems. Similarly, the initial conditions have been further changed and different co-existing attractors are obtained. The blue colour double scroll chaotic attractor is obtained at the initial conditions $(m^*, x^*, y^*, z^*) = (0.8, 0.3, 0, 0)$. The red-colour boundary periodic attractor is obtained at the initial conditions $(m^*, x^*, y^*, z^*) = (0.8, 0.6, 0, 0)$ (figure 8). Similarly, if we changed different sets of initial conditions, then the system may give different dynamics.
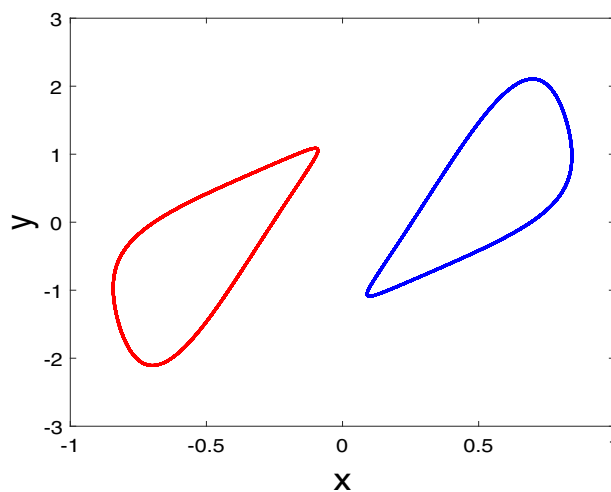


**Figure 7.** Symmetry property: Phase portraits of the two sets of initial conditions.
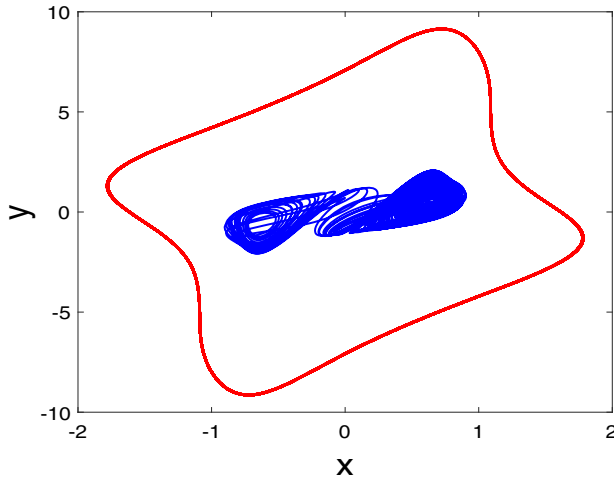
**Figure 8.** Multistability: Phase portraits of the two sets of initial conditions are re-plotted. The blue colour represents the chaotic double-scroll attractor and the red colour indicates the boundary periodic attractor.

## 4. Controller design and numerical simulations

In this section, the memristive Chua circuit (MCC) is demonstrated with fractional scanning. This analysis confirmed that for different sets of fractional values, the trajectories settle in different time limits. The controlled FO memristive system with control output is programmed as

$$
\begin{cases}
\dot{m}^{q_1} = \hat{\alpha}[y - m + W(w)m] + u_1 \\
\dot{y}^{q_2} = m - y - z + u_2 \\
\dot{z}^{q_3} = \beta y + u_3 \\
\dot{w}^{q_4} = -\rho m - \epsilon w + u_4,
\end{cases} \tag{11}
$$

where $u_1$, $u_2$, $u_3$ and $u_4$ are control inputs. Now, we consider fractional order $\alpha = \max\{q_1, q_2, q_3, q_4\}$. Moreover, we extend the subsequent MCC model with the switching rules:

$$
\dot{x}^\alpha(t) = \mathcal{A}_{\sigma(t)} x(t) + \mathcal{B}_{\sigma(t)} u(t), \tag{12}
$$

where

$$
\mathcal{A}_{\sigma(t)} =
\begin{bmatrix}
\hat{\alpha}(-1 + W(w)) & \hat{\alpha} & 0 & 0 \\
1 & -1 & -1 & 0 \\
0 & \beta & 0 & 0 \\
-\rho & 0 & 0 & -\epsilon
\end{bmatrix},
$$

$$
\mathcal{B}_{\sigma(t)} =
\begin{bmatrix}
1 & 0 & 0 & 0 \\
0 & 1 & 0 & 0 \\
0 & 0 & 1 & 0 \\
0 & 0 & 0 & 1
\end{bmatrix},
$$

$x = [m, y, z, w]^T \in \mathbb{R}^n$, $u = [u_1, u_2, u_3, u_4] \in \mathbb{R}^n$.

In light of the connection of the memristor in (11), $w$ is intended to deliver the two modes (switching), where

$$
\dot{x}^\alpha(t) =
\begin{cases}
\mathcal{A}_1 x(t) + \mathcal{B}_1 u(t), & |w| \leq 1, \\
\mathcal{A}_2 x(t) + \mathcal{B}_2 u(t), & |w| > 1.
\end{cases} \tag{13}
$$

Here,

$$
\mathcal{A}_1 =
\begin{bmatrix}
-\hat{\alpha} + \hat{\alpha}a & \hat{\alpha} & 0 & 0 \\
1 & -1 & -1 & 0 \\
0 & \beta & 0 & 0 \\
-\rho & 0 & 0 & -\epsilon
\end{bmatrix},
$$

$$
\mathcal{A}_2 =
\begin{bmatrix}
-\hat{\alpha} + \hat{\alpha}b & \hat{\alpha} & 0 & 0 \\
1 & -1 & -1 & 0 \\
0 & \beta & 0 & 0 \\
-\rho & 0 & 0 & -\epsilon
\end{bmatrix},
$$

$$
\mathcal{B}_1 = \mathcal{B}_2 =
\begin{bmatrix}
1 & 0 & 0 & 0 \\
0 & 1 & 0 & 0 \\
0 & 0 & 1 & 0 \\
0 & 0 & 0 & 1
\end{bmatrix},
$$

where $a > 0$, $b > 0$ are constants. Equation (13) can also be addressed as a linear uncertain system:

$$
\dot{x}^\alpha(t) = \mathcal{A}(\theta) x(t) + \mathcal{B}(\theta) u(t). \tag{14}
$$

Using the assigned rule

$$
\theta_1 =
\begin{cases}
1, & |w| \leq 1, \\
0, & |w| > 1,
\end{cases}
\qquad
\theta_2 =
\begin{cases}
0, & |w| \leq 1, \\
1, & |w| > 1,
\end{cases}
$$

where $\mathcal{A}(\theta)$ and $\mathcal{B}(\theta)$ are matrices with the uncertainty of the real parameter $\theta_i$ and fulfill the real convex polytopic approach, that is, $[\mathcal{A}(\theta) \quad \mathcal{B}(\theta)] \in \Omega$, where

$$
\Omega = \left\{ [\mathcal{A}(\theta) \, \mathcal{B}(\theta)] := \sum_{i=1}^{2} \theta_i [\mathcal{A}_i \, \mathcal{B}_i], \, \theta_i \geq 0, \right.
$$

$$
\left. \sum_{i=1}^{2} \theta_i = 1 \right\}. \tag{15}
$$

Initially, we will give valuable definitions and lemmas to prove the following theorem.

### DEFINITION 1 [22]

The Riemann–Liouville fractional integral operator of order $\alpha > 0$ of a function $f(t)$ is denoted by

$$
\mathcal{J}_t^\alpha f(t) = \frac{1}{\hat{\Gamma}(\alpha)} \int_0^t (t - \theta)^{\alpha-1} f(\theta) \, d\theta, \tag{16}
$$

where $\hat{\Gamma}(\cdot)$ is the gamma function,

$$
\hat{\Gamma}(\theta) = \int_0^\theta e^{-t} t^{\theta-1} dt, \quad \theta > 0.
$$

The Riemann–Liouville derivative of order $\alpha \in (0, 1)$ is accordingly defined as

$$\mathcal{D}_R^\alpha f(t) = \frac{\mathrm{d}}{\mathrm{d}t}(\mathcal{I}_t^{1-\alpha} f(t)).$$

## DEFINITION 2 [22]

The Caputo fractional derivative of order $\alpha \in (0, 1)$ is defined by

$$\mathcal{D}_t^\alpha f(t) = \mathcal{D}_R^\alpha(f(t) - f(0)), \ t \geq 0.$$

*Lemma 1 [52]. Consider $x(t)$ be a real-valued continuous function then*

$$\mathcal{I}_t^\alpha(\mathcal{D}_t^\alpha x(t)) = x(t) - x(0), \ \alpha \in (0, 1).$$

*Lemma 2 [53]. Consider $x(t) \in \mathbb{R}^n$ as a continuous and derivable function. Then, the subsequent inequality holds for any $t \geq t_0$,*

$$\frac{1}{2}\mathcal{D}_t^\alpha(x^T(t)\mathcal{P}x(t)) \leq x^T(t)\mathcal{P}\mathcal{D}_t^\alpha x(t),$$

$$\forall \alpha \in (0, 1), \forall t \geq t_0 \geq 0,$$

*where $\mathcal{P} > 0 \in \mathbb{R}^{n \times n}$ denotes the symmetric matrix.*

*Lemma 3 [54]. Assume that $x, y, z : \mathbb{R}^n$ are non-decreasing and $x(0) = y(0) = 0, v(\cdot)$ is strictly increasing. If there exist $q > 1$ and a continuous function $V(\cdot) : \mathbb{R}^+ \times \mathbb{R}^n \to \mathbb{R}^+$ such that*

   (i) $u(||x||) \leq V(t, x) \leq v(||x||), t \geq 0, x \in \mathbb{R}^n$ and
   (ii) $\mathcal{D}_t^\alpha t V(t, x(t)) \leq -w(||x(t)||)$ if $V(t + s, x(t + s)) < qV(t, x(t)), \forall s \in [-h, 0], t \geq 0$, then the fractional-order system $\mathcal{D}_t^\alpha(t) = f(t, x(t))$ is asymptotically stable.

The FO LPV model is given in the subsequent model:

$$\mathcal{D}_t^\alpha x(t) = \sum_{i=1}^{2} \theta_i[(\mathcal{A}_i + \Delta\mathcal{A}_i)x(t) + (\mathcal{B}_i + \Delta\mathcal{B}_i)u(t)],$$
$$(17)$$

where $\alpha \in (0, 1)$, $x(t) \in \mathbb{R}^n$ and $u(t) \in \mathbb{R}^m$ are the state and control input vectors, respectively and $\mathcal{A}_i$, $\mathcal{B}_i$ are input matrices with compatible dimensions. $\Delta\mathcal{A}_i(t) = \hat{E}_1\hat{F}_1(t)\hat{H}_1$, $\Delta\mathcal{B}_i(t) = \hat{E}_2\hat{F}_2(t)\hat{H}_2$, where $\hat{E}_1, \hat{H}_1, \hat{E}_2, \hat{H}_2$ are known real constant matrices with proper dimensions. $\hat{F}_1(t)$ *and* $\hat{F}_2(t)$ are unknown real-time varying matrices that fulfill $\hat{F}_1^T(t)\hat{F}_1(t) \leq I, \hat{F}_2^T(t)\hat{F}_2(t) \leq I, \forall t \geq 0$.

Related to this framework is the accompanying cost function:

$$\mathcal{J}(u) = \frac{1}{\hat{\Gamma}(\alpha)}\int_0^{\mathcal{T}_f}[x^T(s)\mathcal{Q}_1 x(s) + u^T(s)\mathcal{Q}_3 u(s)]\mathrm{d}s,$$
$$\forall \mathcal{T}_f > 0. \qquad (18)$$

## DEFINITION 3 [41]

Under the control law $u^*(t) = \mathcal{K}_i x(t)$ and a positive number $J^*$ with the end goal that the closed-loop system achieves

$$\mathcal{D}_t^\alpha x(t) = \sum_{i=1}^{2} \theta_i[(\mathcal{A}_i + \Delta\mathcal{A}_i + \mathcal{B}_i\mathcal{K}_i + \Delta\mathcal{B}_i\mathcal{K}_i)x(t)],$$
$$(19)$$

asymptotically stable and fulfills $J(u^*) \leq J^*$, such that $J^*$ is a guaranteed cost value and the suggested control $u^*(t)$ is supposed to be a guaranteed cost controller.

### 4.1 Control results

The accompanying theorem builds up a principle with respect to LMIs for the issue of guaranteed cost control of uncertain FO systems by using the Razumikhin theorem approach.

**Theorem 1.** *Consider* (19) *along with the cost function* (18). *For given symmetric matrices $Q_1 > 0$, $Q_2 > 0$, $Q_3 > 0$, $u(t) = \mathcal{Y}_i \mathcal{P}^{-1} x(t)$ is a guaranteed cost controller for* (19), *if there exists a symmetric matrix $\mathcal{P} > 0$, a matrix $\mathcal{Y}_i$ with suitable dimensions, scalars $\epsilon_a > 0, \epsilon_b > 0$ and satisfying the subsequent LMIs:*

$$\Omega = \begin{bmatrix} E_{11} & \mathcal{P}H_1 & \mathcal{Y}_i^T H_2^T & \mathcal{P}Q_2 & \mathcal{Y}_i^T Q_3^T \\ * & -\varepsilon_a I & 0 & 0 & 0 \\ * & * & -\varepsilon_b I & 0 & 0 \\ * & * & * & -Q_1 & 0 \\ * & * & * & * & -Q_3 \end{bmatrix} < 0. \qquad (20)$$

*Furthermore, the cost of system* (19) *is defined by $n = J^* = \lambda_{\max}(\mathcal{P}^{-1})||\phi||^2$, where*

$$E_{11} = \mathcal{A}_i\mathcal{P} + \mathcal{P}\mathcal{A}_i^T + \mathcal{B}_i\mathcal{Y}_i + \mathcal{Y}_i^T\mathcal{B}_i^T$$
$$+ \epsilon_a E_1 E_1^T + \epsilon_b E_2 E_2^T.$$

*Proof.* Consider the non-negative quadratic function (see [41]):

$$V(x(t)) = x^T(t)\mathcal{P}^{-1}x(t).$$

It is easy to verify that

$$\lambda_{\min}(\mathcal{P}^{-1})||x(t)||^2 \leq V(t, x(t)) \leq \lambda_{\max}(\mathcal{P}^{-1})||x(t)||^2.$$

In this manner, Lemma 3, condition (i) is fulfilled. It follows from Lemma 2 that we get the $\alpha$-order ($0 < \alpha < 1$) Caputo derivative of $V(x(t))$ with (19) as follows:

$$\mathcal{D}_t^\alpha V(x(t))$$
$$\leq 2x^T(t)P^{-1}\mathcal{D}_t^\alpha x(t)$$
$$= 2x^T(t)\mathcal{P}^{-1}[(\mathcal{A}_i + \Delta\mathcal{A}_i(t) + \mathcal{B}_i\mathcal{K}_i + \Delta\mathcal{B}_i(t)\mathcal{K}_i)]$$
$$= 2x^T(t)[\mathcal{P}^{-1}\mathcal{A}_i + \mathcal{P}^{-1}\Delta\mathcal{A}_i(t)\mathcal{P}^{-1}\mathcal{B}_i\mathcal{K}_i$$

$$+ \mathcal{P}^{-1} \Delta \mathcal{B}_i(t) \mathcal{K}_i]$$
$$= x^T(t) \big[ \mathcal{P}^{-1} \mathcal{A}_i + \mathcal{A}_i^T \mathcal{P}^{-1} + \mathcal{P}^{-1} \mathcal{B}_i \mathcal{K}_i$$
$$+ K^T \mathcal{B}_i^T \mathcal{P}^{-1} \big] x(t) + 2 x^T(t) P^{-1} E_1 F_1(t) H_1 x(t)$$
$$+ 2 x^T(t) \mathcal{P}^{-1} E_2 F_2(t) H_2 \mathcal{K}_i x(t). \tag{21}$$

Using the Cauchy matrix inequality, we have the accompanying evaluations.

$$2 x^T(t) \mathcal{P}^{-1} E_1 F_1(t) H_1 x(t)$$
$$\leq \epsilon_a x^T(t) \mathcal{P}^{-1} E_1 E_1^T \mathcal{P}^{-1} x(t)$$
$$+ \epsilon_a^{-1} x^T(t) H_1^T H_1 x(t),$$
$$2 x^T(t) \mathcal{P}^{-1} E_2 F_2(t) H_2 \mathcal{K}_i x(t)$$
$$\leq \epsilon_b x^T(t) \mathcal{P}^{-1} E_2 E_2^T \mathcal{P}^{-1} x(t)$$
$$+ \epsilon_b^{-1} x^T(t) \mathcal{K}_i^T H_2^T H_2 \mathcal{K}_i x(t). \tag{22}$$

Therefore, we obtain

$$\mathcal{D}_t^\alpha V(x(t))$$
$$\leq x^T(t) \big[ \mathcal{P}^{-1} A + A^T \mathcal{P}^{-1} + \mathcal{P}^{-1} B K$$
$$+ \mathcal{K}_i^T B^T \mathcal{P}^{-1} + \epsilon_a \mathcal{P}^{-1} E_1 E_1^T \mathcal{P}^{-1}$$
$$+ \epsilon_a^{-1} H_1^T H_1 + \epsilon_b \mathcal{P}^{-1} E_2 E_2^T \mathcal{P}^{-1}$$
$$+ \epsilon_b^{-1} \mathcal{K}_i^T H_2^T H_2 \mathcal{K}_i + (Q_1 + \mathcal{K}_i^T Q_3 \mathcal{K}_i) \big] x(t), \tag{23}$$

pre and post multiplying by $\mathcal{P}$ by the above inequality and introducing $\mathcal{K}_i = \mathcal{Y}_i \mathcal{P}^{-1}$, we have

$$\mathcal{D}_t^\alpha V(x(t))$$
$$\leq x^T(t) \big[ A\mathcal{P} + \mathcal{P}A^T + B\mathcal{Y}_i$$
$$+ \mathcal{Y}_i^T B^T + \epsilon_a E_1 E_1^T$$
$$+ \epsilon_a^{-1} \mathcal{P} H_1^T H_1 \mathcal{P} + \epsilon_b E_2 E_2^T$$
$$+ \epsilon_b^{-1} \mathcal{Y}_i^T H_2^T H_2 \mathcal{Y}_i + (\mathcal{P} Q_1 \mathcal{P} + \mathcal{Y}_i^T Q_3 \mathcal{Y}_i) \big] x(t)$$
$$\leq x^T(t) \Omega x(t). \tag{24}$$

Using the Schur complement lemma, we get $\Omega < 0$, corresponding to LMI (20), to get

$$\mathcal{D}_t^\alpha V(x(t)) < 0, \forall t \geq 0. \tag{25}$$

Along these lines, Lemma 3, condition (ii) is additionally fulfilled. Therefore, the closed-loop system is asymptotically stable. Furthermore, we will evaluate the guaranteed cost function (21). From conditions (20) and (24), we have the following.

$$\mathcal{D}_t^\alpha V(x(t)) < -x^T(t)(Q_1 + \mathcal{K}_i^T Q_3 \mathcal{K}_i) x(t),$$
$$\forall t \in [0, t_f]. \tag{26}$$

Integrating (26) with order $\alpha$ on both sides of 0 to $t_f$ and using Lemma 1, we obtain the following result:

$$V(x(T_f)) \leq V(x(0)) - J(u). \tag{27}$$

Therefore,

$$J(u) \leq V(x(0)) \leq \lambda_{\max}(\mathcal{P}^{-1}) \|\phi\|^2 = J^*, \tag{28}$$

as $V(x(T_f)) = x^T(T_f) \mathcal{P}^{-1} x(T_f) \geq 0$. This completes the proof.

## 5. Simulation results

Let

$$\mathcal{D}_t^\alpha x(t) = \sum_{i=1}^{2} \theta_i [(\mathcal{A}_i + \Delta \mathcal{A}_i + \mathcal{B}_i \mathcal{K}_i + \Delta \mathcal{B}_i \mathcal{K}_i) x(t)], \tag{29}$$

where $0 < a < 1, 0 < b < 1$ and

$$\mathcal{A}_1 = \begin{bmatrix} 7.2 & 12 & 0 & 0 \\ 1 & -1 & -1 & 0 \\ 0 & 28 & 0 & 0 \\ -37 & 0 & 0 & -12 \end{bmatrix},$$

$$\mathcal{A}_2 = \begin{bmatrix} -10.08 & 12 & 0 & 0 \\ 1 & -1 & -1 & 0 \\ 0 & 28 & 0 & 0 \\ -37 & 0 & 0 & -12 \end{bmatrix},$$

$\mathcal{B}_1 = \mathcal{B}_2 = I_4$, $H_1 = \text{diag}\{0.1, 0.1, 0.1, 0.1\}$, $H_2 = \text{diag}\{0.2, 0.2, 0.2, 0.2\}$, $E_1 = 0.1$, $E_2 = 0.1$.

To stabilise the uncertain FO LPV system (20) under consideration, we design the controller $\mathcal{K}_i = \mathcal{Y}_i P^{-1}$ with the parameters given above. For this reason, addressing the LMIs in Theorem 1 with the given parameters using the Matlab LMI toolbox, we acquire the accompanying gain matrices

$$\mathcal{K}_1 = \begin{bmatrix} -9.6093 & -2.5499 & -0.4027 & 6.5997 \\ -2.4547 & -5.7844 & -5.3641 & 1.1406 \\ -0.4199 & -5.3742 & -5.8989 & -0.3217 \\ 6.2770 & 1.1173 & -0.3527 & -4.7170 \end{bmatrix},$$

$$\mathcal{K}_2 = \begin{bmatrix} -9.1780 & -2.4412 & -0.3841 & 6.3216 \\ -2.5662 & -5.8157 & -5.3704 & 1.2179 \\ -0.3677 & -5.3620 & -5.8984 & -0.3579 \\ 6.7169 & 1.2364 & -0.3328 & -5.0231 \end{bmatrix}.$$

The controlling strategies were applied in various combinations of fractional order of the system equation. The control parameters were kept constant and the functionalities could be varied to understand the dynamic changes of fractional orders in the system.

Figure 9 shows the phase portraits and time series with different variables. The oscillations are purely chaotic and oscillate asymptotically without applying any control strategies (uncontrolled).

Figure 10 shows the control response of system (29) by varying the fractional order $q_4$ with two sets of values
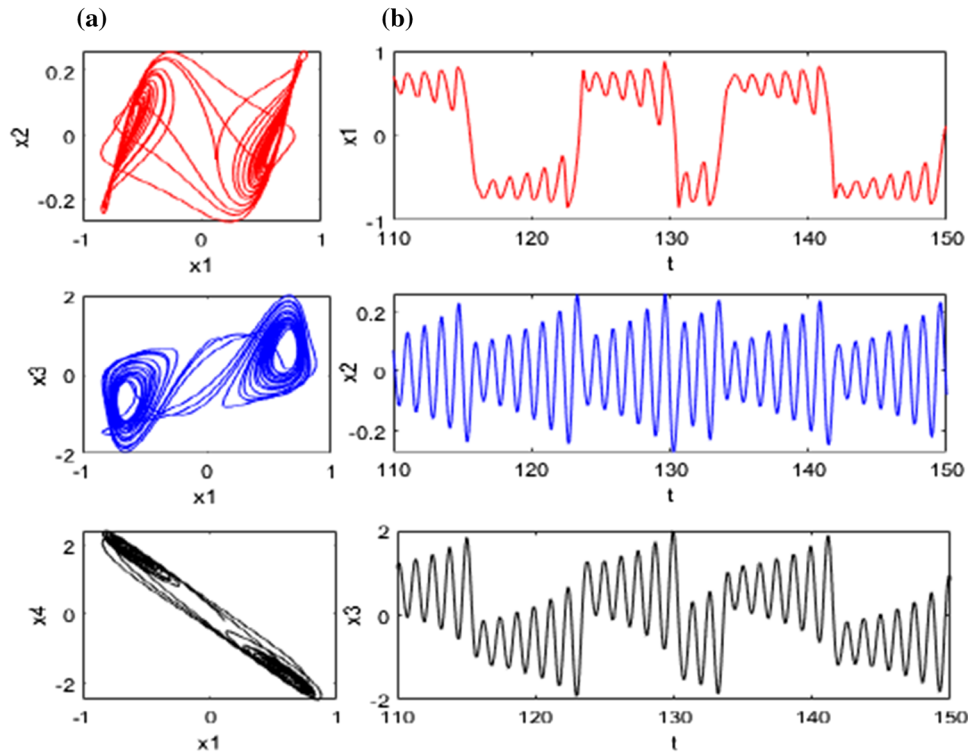
**Figure 9.** Numerically computed (**a**) phase portraits and (**b**) time series of chaotic oscillation without controlling. The fractional orders are fixed as $q_1, q_2, q_3, q_4 = (1, 1, 1, 0.9)$.

$q_4 = 0.4$ and $q_4 = 0.7$ and the rest of fractional orders, i.e., $q_1, q_2, q_3$ have been considered as one (integer). From figure 10, it is clearly seen that when the fractional order is gradually decreased, the damping of the system is increased. This can also be visualised by plotting the phase portraits of the variables. Figure 11 shows the phase portraits of the controlling variables $x_1$ and $x_2$ by plotting the phase portraits between them. Here, three sets of fractional order $q_4$ are varied. From the visuals of figure 11, the controlling is one-to-one related to fractional orders. The stable point (zero) is denoted as a pink circle in the figure.

Similarly, the other fractional orders $(q_1, q_2, q_3)$ could be varied and for the sake of simplicity, these plots are avoided here.

## 6. Importance and future direction

Studying the FO-based nonlinearity gives more insight/advantages in understanding the fractional complex system. The importance of the present study is as follows

- The main characteristics of memristor-based dynamical systems used in different domains is their memory outcome (history dependence). However, the FO nonlinearity-based memristor system gives more features than traditional complex systems.
- In the modified Chua's circuit, the dimension of chaoticity can be defined by measuring DC representing the counting box fractional dimension of chaotic flows. In the context of nanoscience, which is devoted to numerically exploring electronic circuits, the reported norms support the usefulness of the modified Chua's circuit for emulating fractional emergent phenomena. Because the memristor exclusively has the purpose of a time-dependent nonlinear element, as a time-independent linear element, it decreases to a regular resistor.
- The FO-based memristor systems in the form of single, coupled and network of arrangements which may give high degree of freedom and large memory property. Moreover, this FO nonlinearity system gives the framework for more efficient circuit modelling and control in various fields.
- FO-based micro- and nanoelectronic devices can be made for appropriate applications with notable accuracies to avoid failures/errors. Moreover, the microstructures have supercapacitors with nanocrystalline and microcrystalline surfaces, which are deposited electrodes. It can be modelled more successfully by FO equations than by classic models.
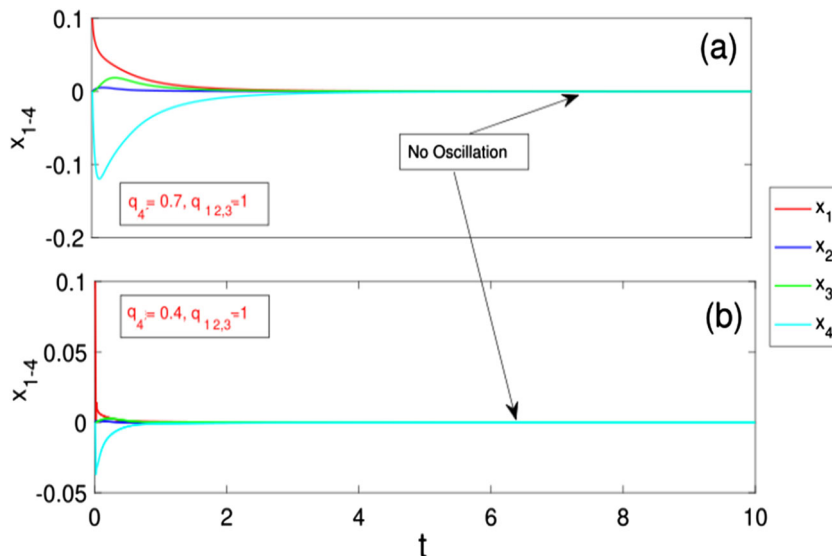
**Figure 10.** Control response of system (29). The fractional order is varied for (**a**) $q_4 = 0.7$ and (**b**) $q_4 = 0.4$. The fractional orders are fixed at $q_1, q_2, q_3 = 1.0$. Different colours indicate the state variables ($x_{1,2,3,4}$) of the system.
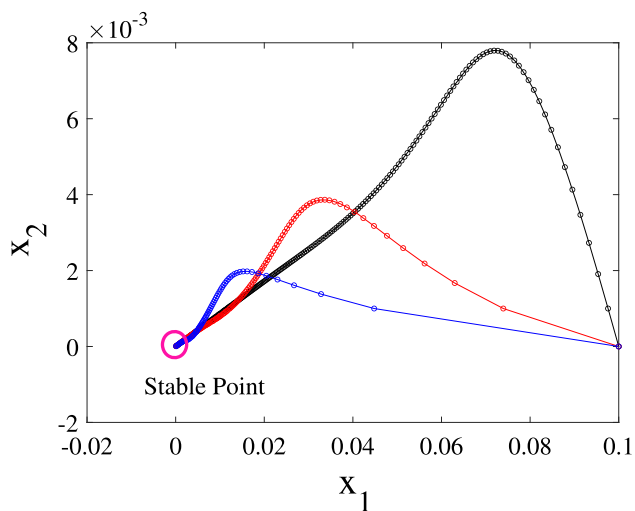


**Figure 11.** Numerical phase portraits of ($x_1$–$x_2$) variables with respect to different FO values. $q_4 = 0.8$ (black dotted line), $q_4 = 0.6$ (red dotted line) and $q_4 = 0.4$ (blue dotted line). Here, the stable points are identified with the pink circle.

- This method appears very promising in FO systems studied in different fields such as electrical science, electrochemistry, control science, diffusion process, viscoelasticity, material science, etc.

In the future, fractional memristor nonlinearity will be studied using a coupled network of oscillators and will demonstrate the important features of both hidden and self-excited attractors. This study will show the large-memory property. In particular, fractional memristive nonlinearity will be investigated by coupled and network systems with the shared nonlinearity concepts.

## 7. Conclusions

We investigated the least FO nonlinearity to generate chaos in a memristor-based Chua FO system. The memristor-based fractional Chua system is considered and we found the existence of chaos for least-order nonlinearity at $q_4 = 0.48$. Several numerical and experimental analyses were performed. For global dynamics of the system, the two-parameter scanning is performed between FO nonlinearity vs. fractional-state variables. The oscillatory limits and the multistability phenomenon were identified by the two-parameter plot. To the best of the author's knowledge, this is the first study to perform FO nonlinearity in hidden and self-excited systems to find the minimal strength of nonlinearity to produce chaos.

Moreover, we handle the guaranteed cost controller method for MCC models with parameter uncertainties. Primarily, an uncertain MCC model is construed as a linear uncertainty system in terms of the function of the memristor. The proposed plan can be utilised to deal with the constant use of MCC models. By building an appropriate Lyapunov functional and utilising inequality techniques, the asymptotic stability of the addressed model has been set up as far as LMIs are concerned. Moreover, the control gain matrices are determined by tackling a set of LMIs using the MATLAB LMI control toolbox. Finally, the simulation results verify the established theoretical findings. The strategy in this work can be utilised to manage more complicated issues, for example, filtering design [55], observer design, external disturbances (dissipativity, passivity, $H_\infty$ performance [56]) and event-triggered

scheme [57–59] to save the limited network communication bandwidth.

## Acknowledgements

## References

[1] D B Strukov, G S Snider, D R Stewart and R S Williams, *Nature* **453**, 80 (2008)

[2] R Kozma, R E Pino and G E Pazienza, *IEEE Access* **4**, (2012)

[3] A Adamatzky and L Chua, *Memristor networks* (Springer Science & Business Media, 2013)

[4] H Xi and R Zhang, *Chin. J. Phys.* **77**, 572 (2022)

[5] P K Sharma, R K Ranjan, F Khateb and M Kumngern, *IEEE Access* **08**, 171397 (2020)

[6] Y Chen, Q Cao, Z Zhu, Z Wang and Z Zhao, *IEEE Access* **9**, 44402 (2021)

[7] L Chua, *IEEE Trans. Circuit Theory* **18**, 507 (1971)

[8] R Stanley Williams, How we found the missing memristor, in: *Chaos, CNN, memristors and beyond* (World Scientific, 2013) pp. 483–489

[9] R Tetzlaff, *Memristors and memristive systems* (Springer, 2013)

[10] C Li, M Wei and J Yu, *Int. Conference on Communications, Circuits and Systems* (2009) p. 944

[11] B Muthuswamy, *Int. J. Bifurc. Chaos* **20**, 1335 (2010)

[12] V T Pham, S Jafari, S Vaidyanathan, C Volos and X Wang, *Sci. China Technol. Sci.* **59**, 358 (2016)

[13] S Sabarathinam, A Prasad, *AIP Conf. Proc.* **1942**(**1**), 060025 (2018)

[14] S Sabarathinam and K Thamilmaran, *AIP Conf. Proc.* **1832**(**1**), 060007 (2017)

[15] I E Ebong and P Mazumder, *IEEE Trans. Nanotechnol.* **10**, 1454 (2011)

[16] M A Zidan, H A H Fahmy, M M Hussain and K N Salama, *Microelectron. J.* **44**, 176 (2013)

[17] R Jothimurugan, S Sabarathinam, K Suresh and K Thamilmaran, *Advances in memristors, memristive devices and systems* (Springer, 2017) pp. 343–370

[18] N Gunasekaran, S Srinivasan, G Zhai and Q Yu, *IEEE Access* **9**, 25648 (2021)

[19] V Varshney, S Sabarathinam, K Thamilmaran, M D Shrimali and A Prasad, *Nonlinear dynamical systems with self-excited and hidden attractors* (Springer, 2021) pp. 327–344

[20] Y Cao, W Jiang and J Wang, *Knowl.-Based Syst.* **233**, 107539 (2021)

[21] I Petráš, Fractional-order systems, in: *Fractional-order nonlinear systems* (Springer Science & Business Media, 2011) pp. 43–54

[22] J Sabatier, O P Agrawal and J A T Machado, Advances in fractional calculus, in: *Theoretical developments and applications in physics and engineering* (Springer, 2007) Vol. 4

[23] D Baleanu, J Machado and A CJ Luo, *Fractional dynamics and control* (Springer Science & Business Media, 2011)

[24] R L Magin, *Crit. Rev. Biomed. Eng.* **32**, 195 (2004)

[25] V T Mai and C H Dinh, *J. Syst. Sci. Complex.* **32**, 1479 (2019)

[26] W Ahmad, R El-Khazali and A S Elwakil, *Electron. Lett.* **37**, 1110 (2001)

[27] D-Y Xue and C-N Zhao, *IET Control. Theory Appl.* **5**, 771 (2007)

[28] I Podlubny, *IEEE Trans. Autom. Control* **44**, 208 (1999)

[29] H-B Bao and J Cao, *Neural Netw.* **63**, 1 (2015)

[30] Y Gu, Hu Wang and Y Yu, *J. Franklin Inst.* **357**, 8870 (2020)

[31] J Palanivel, K Suresh, S Sabarathinam and K Thamilmaran, Chaos Solitons Fractals **95**, 33 (2017)

[32] I Grigorenko and E Grigorenko, *Phys. Rev. Lett.* **91**, 034101 (2003)

[33] CA Monje, B M Vinagre, V Feliu and Y Chen, *Control Eng. Pract.* **16**, 798 (2008)

[34] K Xu, L Chen, M Wang, A M Lopes, M JA Tenreiro and H Zhai, *Mathematics* **8**, 326 (2020)

[35] L Chen, T Li, R Wu, A M Lopes, J A T Machado and K Wu, *Comput. Appl.* **39**, 1 (2020)

[36] M V Thuan, T N Binh and D C Huong, *Asian J.* **22**, 696 (2020)

[37] L Chen, R Wu, L Yuan, L Yin, Y Q Chen and S Xu, *Optim. Control Appl. Meth.* **42**, 1102 (2021)

[38] Vc N Phat, M V Thuan and T N Tuan, *Vietnam J. Math.* **47**, 403 (2019)

[39] L Liu, Y Di, Y Shang, Z Fu and B Fan, *Circuits Syst. Signal Process.* 1 (2021)

[40] D C Huong, *Circuits Syst. Signal Process.* **40**, 4759 (2021)

[41] M V Thuan and D C Huong, *Optim. Control Appl. Methods* **40**, 613 (2019)

[42] H-B Bao and J-D Cao, *Neural Netw.* **63**, 1 (2015)

[43] L Chen, R Wu, J Cao and J-B Liu, *Neural Netw.* **71**, 37 (2015)

[44] G Velmurugan, R Rakkiyappan and J Cao, *Neural Netw.* **73**, 36 (2016)

[45] R Scherer, S L Kalla, Y Tang and J Huang, *Comput. Math. Appl.* **62**, 902 (2011)

[46] N Heymans and I Podlubny, *Rheol. Acta* **45**, 765 (2006)

[47] Y Luchko and R Gorenflo, *Frac. Calc. Appl. Anal.* **1**, 63 (1998)

[48] W M Ahmad and J C Sprott, *Chaos Solitons Fractals* **16**, 339 (2003)

[49] BM Vinagre, I Podlubny, A Hernandez and V Feliu, *Fract. Calc. Appl.* **3**, 231 (2000)

[50] Z-M Ge and C-Y Ou, *Chaos Solitons Fractals* **34**, 262 (2007)

[51] S Sabarathinam and A Prasad, *AIP Conf. Proc.***1942**, 060025 (2018)

[52] I Podlubny, *Fractional differential equations – An introduction to fractional derivatives, fractional differential equations, to methods of their solution and some of their applications* (Elsevier Academic Press, 1998)

[53] M A Duarte-Mermoud, N Aguila-Camacho, J A Gallegos and R Castro-Linares, *Commun. Nonlinear Sci. Numer. Simul.* **22**, 650 (2015)

[54] Y Wen, X-F Zhou, Z Zhang and S Liu, *Nonlinear Dyn.* **82**, 1015 (2015)

[55] R Vadivel, R Suresh, P Hammachukiattikul, B Unyong and N Gunasekaran, *IEEE Access* **9**, 145133 (2021)

[56] R Anbuvithya, S S Dheepika, R Vadivel, N Gunasekaran and P Hammachukiattikul, *IEEE Access* **9**, 31454 (2021)

[57] R Vadivel, M S Ali and F Alzahrani, *Chin. J. Phys.* **60**, 68 (2019)

[58] M Syed Ali, R Vadivel and K Murugan, *Chin. J. Phys.* **56**, 2448 (2018)

[59] D C Huong, *Optimal control applications and methods* (Wiley Online Library, 2022)